



## Automated pollen recognition using 3D volume images from fluorescence microscopy

Olaf Ronneberger<sup>1</sup>, Eckart Schultz<sup>2</sup> & Hans Burkhardt<sup>3</sup>

<sup>1</sup>German Weather Service, Freiburg, Germany (E-mail: Olaf@Ronneberger.net); <sup>2</sup>German Weather Service, Freiburg, Germany (E-mail: Eckart.Schultz@dwd.de); <sup>3</sup>Computer Science Department, University of Freiburg, Germany (E-mail: Hans.Burkhardt@informatik.uni-freiburg.de)

Received 2 February 2001; accepted in final form 17 June 2002

**Key words:** airborne pollen, automatic recognition, fluorescence microscopy, gray scale invariants, image processing, pattern recognition, volume image data

### Abstract

Identifying and counting of pollen grains in ambient air samples is still a demanding and time-consuming task even for an experienced microscopist. This article describes a technique which may be employed to establish a fully automated system for this task. Based on a 3D volume fluorescence image of a pollen grain taken with a confocal laser scanning microscope, the described system is able to recognize the pollen taxa. The system autonomously extracts all required information for the recognition from a data base with reference objects (self-learning system) and only needs to calculate very general purpose features of the volumetric data sets (so-called gray scale invariants). This allows for easy adaptation of the system to other conditions (e.g., pollen of a special area) or even other objects than pollen (e.g., spores, bacteria etc.) just by exchanging the reference data base. When using a reference data base with the 26 most important German pollen taxa, the recognition rate is 92%. With a special database for allergic purposes recognizing only *Corylus*, *Alnus*, *Betula*, *Poaceae*, *Secale*, *Artemisia* and “allergically non-relevant” the recognition rate is 97.4%.

**Abbreviations:** LSM – Laser Scanning Microscope; SVM – Support Vector Machine; FFT – Fast Fourier Transform; pixel – picture element; voxel – volume element

### 1. Introduction

Pollen counting is still done by eye. This routine work is a demanding and time consuming task even for experienced microscopists. For the conventional measurement the pollen are sampled with the Burkard trap. The microscopic samples are not available earlier than the next day. The quality and reliability of these routine data vary considerably according to the motivation and qualification of the pollen counters.

These well known limitations of real-world pollen data gave reason for a joint project of the German Weather Service and the MeteoSwiss in cooperation with the Institute for Computer Science of the University of Freiburg in order to develop a computer based

technique for automatic pollen recognition based on image recognition techniques. This automated pollen recognition should provide reproducible data with known quality and faster availability of the data.

Even though the pattern recognition on images is widely used in several biological applications, there are only very few papers in the literature dealing with pollen recognition, (e.g., Langford et al., 1986; Langford et al., 1990; France et al., 1997) and most of them deal with fossil pollen. To the authors' knowledge, there are only two other recent projects aimed at the automatic identification of airborne pollen with image recognition techniques; one project in Australia, which has already been finished, and one within a joint Italian, French and Spanish EU-project

called "A.S.T.H.M.A". Results of both projects were presented at the "2nd European Symposium on Aerobiology" in Vienna, Austria from 5-9 September 2000.

In contrast to other approaches we decided to employ the following:

1. fluorescence microscopy for imaging the pollen grains
2. the full 3D volumetric data set of each pollen grain recorded with a confocal laser scanning microscope
3. general purpose "gray-scale invariants" for the extraction of features of these volumetric data sets
4. a classifier based on "support vector machines", which automatically learns how to recognize the different pollen taxa from a reference data set of pollen grains.

The employment of the strong primary fluorescence of pollen (McCrone and Delly, 1973) eases their isolation from other components of an air sample (Figure 1). Furthermore fluorescence images are better suited for the subsequent 3D analysis of each pollen grain. Instead of using only 2D views, we record the full 3D information of the objects. This volumetric data was recorded with a confocal laser-scanning microscope, but may also be obtained with a conventional fluorescence microscope and post-processing (so-called deconvolution) of the acquired images.

For the recognition-software we do not use the widespread pollen identification schemes which consist of a step-by-step procedure tailored to meet the needs and the potential of a human identifier. These schemes can be transferred on a computer only with great difficulties.

Therefore we use 3D gray scale invariants, which are able to classify objects independent from their position and orientation in space. These abstract features can be directly calculated from the recorded 3D gray value distribution of the pollen grain.

The classification is done with "support vector machines" which were trained with a reference data base. This "computer-optimized" way of object recognition has several advantages: by simply exchanging the reference data base and retraining the classifier one can adapt the system to special conditions or even use it for objects other than pollen.

## 2. Methods

### 2.1 Sampling and preparation

To set up a reference data base, the pollen grains were directly collected from the plants of interest in order to prepare pure samples of each pollen taxa. This approach ensured that the pollen were correctly labeled. As a limitation it has to be considered that these pollen may have less variations in size and morphology than airborne pollen because the pollen for each taxa were taken just from one plant.

Furthermore our reference pollen are not expected to have deformations due to sampling stress in the Burkard trap and there are no contaminated or agglomerated pollen grains.

The pollen grains were mounted on glass slides and embedded in a 88% glycerine solution suitable for fluorescence microscopy at any wavelength.

Accordingly treated samples were prepared for pollen of the following plant taxa:

*Acer, Artemisia, Alnus, Alnus viridis, Betula, Carpinus, Corylus, Chenopodium, Compositae, Cruciferae, Fagus, Quercus, Aesculus, Juglans, Fraxinus, Plantago, Platanus, Poaceae, Secale, Rumex, Populus, Salix, Taxus, Tilia, Ulmus, Urtica.*

### 2.2 Fluorescence microscopy

For conventional pollen counting translucent microscopy is used. The pollen recognition at ambient air samples is complicated due to the huge variety of particles, which are not only of biological origin (Figure 1a). The strong primary fluorescence of pollen provides an easy accessible feature which allows a reliable isolation from the background and from most other particles (either organic or inorganic) (Figure 1b). We obtained the images of the best signal to noise ratio when using blue excitation light (about 450nm) and recording the green to yellow emission of the pollen grains.

Furthermore fluorescence microscopic recordings have great advantages if reconstructing volumetric data from an image stack (see next section).

### 2.3 3D volume imaging

Even for a human pollen counter it is hard to recognize a pollen of an unfavorable orientation from a single 2D view. As today's computer codes are still by far less capable in object recognition than a human, the identification of all the pollen from a single 2D image

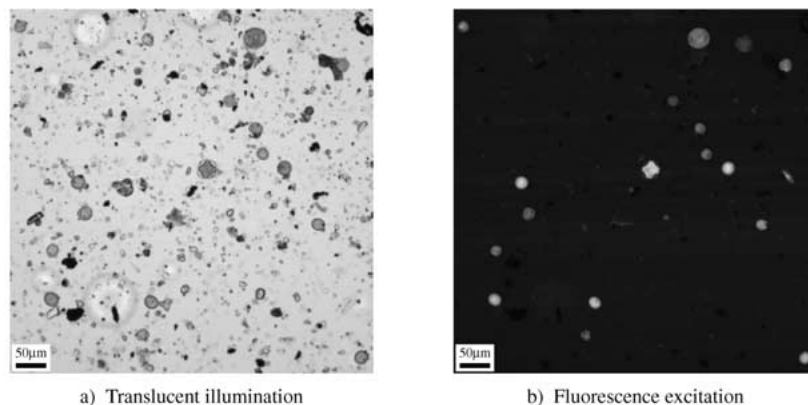


Figure 1. Ambient particle sample collected with a Burkard trap on April 3, 2000 at an urban site in Freiburg recorded with a) translucent and b) fluorescence microscopy. The strong primary fluorescence of pollen grains can be used for a simple and robust selection and segmentation.

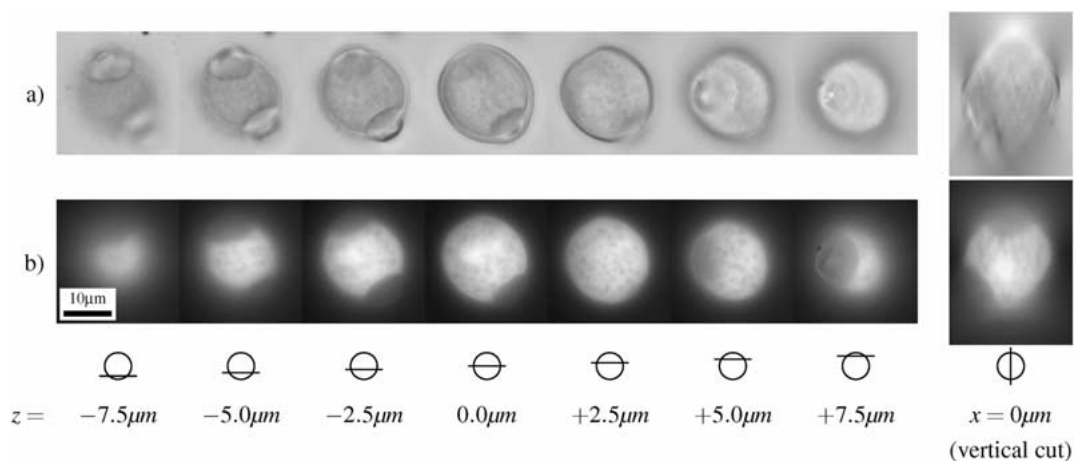


Figure 2. Translucent (a) and fluorescence (b) microscopic images of a *Betula* pollen grain recorded with a 100x oil-objective at different vertical positions. The rightmost image shows a vertical cut through the recorded volume image which was constructed of 256 single images.

is extremely unlikely. This result was also found by Mazière (1997).

To obtain more information, the human focuses onto different focus planes of the pollen grain. Similarly we record several planes in  $z$ -direction and stack them up to a volume image. Translucent microscopy is not well suited for this technique, because the recorded images are the result of a complicated integral of light defraction and refraction due to the inhomogeneities of the refraction coefficient inside the pollen grain and its surrounding.

This effect becomes obvious, when comparing the image from the lower edge ( $z = -7.5\mu\text{m}$ ) and the upper edge ( $z = +7.5\mu\text{m}$ ) of the pollen grain in Figure 2a: The upper edge appears much brighter, because the whole pollen acts as a lens and partly focuses the incoming parallel light on it. This effect can clearly be seen in the vertical cut of the translu-

cent volume image. Furthermore the pollen appears stretched in  $z$ -direction and the upper pore is nearly invisible.

In fluorescence microscopy all fluorescence active molecules of the pollen act as small light sources (Figure 2b). The resulting image therefore can be regarded as the measurement of the local fluorescence activity, which is largely independent from the direction of viewing and the direction of illumination.

A general problem of imaging systems is that the true image of the focused plane of the object is disturbed by the light originating from other object planes, which are out of focus. In order to eliminate the light from these non-focused parts, one can use the confocal microscopy, which eliminates this light by hardware components to provide images with the highest quality but very costly. An alternative are the so-called deconvolution techniques, which remove the

light dispersion by post-processing the digital images taken with a conventional fluorescence microscope. For the development of the recognition software we started with high-quality images from a confocal laser-scan microscope.

To investigate the capabilities of deconvolution techniques, image stacks of some pollen have been recorded with a normal fluorescence microscope and have been subjected to a deconvolution using the point spread function of the imaging system, which had been measured by means of very small fluorescing spheres, so-called “beads”. The algorithm used implements the optimal Wiener-Filter. In contrast to other deconvolution systems we use multiple recordings of the same bead to measure the Signal-to-Noise Ratio for each frequency component. This results in a filter, which is not optimized for a special class of objects, but ensures, that no information is lost due to the filtering process.

#### 2.4 Pattern recognition with gray-scale invariants

The general way of object recognition is first to extract appropriate features from the unknown object and then to start a classification based on the resulting set of parameters, with the aim to find the best match between the parameters of the unknown object and the parameters of the labeled objects in a database.

There are mainly two ways to realize an automatic pattern recognition system. The first is to extract highly abstract features from the images, like the “number of pores”, which means to put all “intelligence” of the software to the feature extraction part. This keeps the classifier very simple, but usually needs high efforts in the development of a big collection of highly object-specific functions, e.g., the pore finder, which must be adapted to every pollen species, or even to each possible orientation of a pore.

The alternative is to keep the feature extraction as general as possible and to use a more sophisticated classifier, which can be trained with given samples from a reference data base. The advantage of such an approach is the easy adaption to different environmental conditions or even other objects just by exchanging the reference data base and rerunning the training program.

A quite simple but very powerful way of a general feature extraction is the calculation of so-called “gray-scale invariants” (Schulz-Mirbach, 1995; Burkhardt and Siggelkow, 2001). The gray-scale invariants do not need any segmentation within the object, but

operate directly on the gray-values of the image. Furthermore they are not limited to two-dimensional image data and can be straightforwardly extended to three-dimensional volumetric data (Schael and Siggelkow, 2000).

The aim of such an invariant feature is the following: The scanned 3D volume data set represents one individual pollen grain, independent of its position and orientation in space. This means, that the 3D volume data set of one individual pollen grain, in all possible positions and orientations (Euclidian motion), represent exactly one equivalence class. An invariant transformation is able to map all representations in the vector space of the equivalence class into one point of the feature space and there represents the intrinsic information of the structure, independent of its position and orientation.

The basic idea for the calculation of these invariants is to take a small non-linear kernel function  $f(\mathbf{X})$  for combining some neighboring pixels<sup>1</sup> or voxels<sup>2</sup> and to integrate the results of this function over all possible representations in the equivalence class.

$$T[f](\mathbf{X}) := \frac{1}{|G|} \int_G f(g\mathbf{X})dg \quad (1)$$

$\mathbf{X}$  : gray-value image

$G$  : transformation group

$|G|$  : number of elements in the transformation group

$g$  : one element of the transformation group

For stiff or at least partially quite stiff objects like pollen, these different representations can be described with a simple euclidian transformation (rotation and translation) of the object:

$$T[f](\mathbf{X}) := \frac{1}{2\pi N} \int_{\vec{x}=\vec{0}}^{\vec{x}_{max}} \int_{\varphi=0}^{2\pi} f(g_{\vec{x},\varphi}\mathbf{X})d\varphi d\vec{x} \quad (2)$$

$\vec{X}_{max}$  : extension of the image

$N$  : number of pixels/voxels in the image

Actually, it is not necessary to transform the full image to all possible representations, instead the kernel function can be appropriately transformed, which considerably speeds up the computation and results in linear complexity of the algorithm. This is illustrated by an example in Figure 3.

A further speedup of this still expensive calculation is done for a special class of kernel functions by using a convolution with the image of a circle (or in 3D a

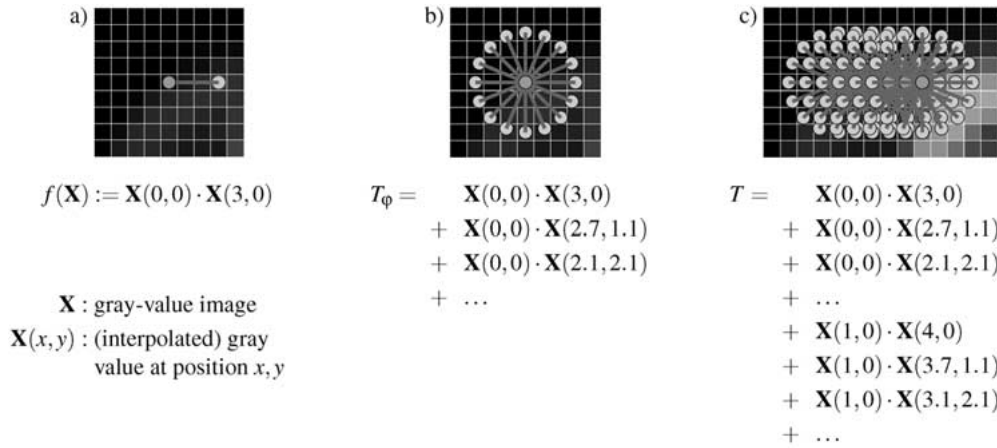


Figure 3. Calculation of a 2D gray-scale invariant: (a) Selection of a non-linear kernel function for combining some neighboring pixels: In this example the kernel function  $f(\mathbf{X})$  is defined as the multiplication of two gray values of distance 3. (b) This kernel function is evaluated for all angles and the results are summed up, to become invariant to rotations of the object. (c) This set of rotated kernel functions is evaluated at all possible positions of the image and the results are summed up, to become invariant to translations of the object. As a result, identical values for  $T$  are obtained independent from the angle and position of the object in the image.

sphere surface) **C**. This convolution may be calculated by means of the Fast Fourier Transform (FFT). For kernel functions of the type

$$f(\mathbf{X}) = a(\mathbf{X}(\vec{0})) \cdot b(\mathbf{X}(\vec{q})) \quad (3)$$

$a, b$  : any functions that transform the gray values  
 $\vec{q}$  : span of the kernel function

one can rewrite Equation 2 for the two-dimensional case using

$$\mathbf{A} := a(\mathbf{X}) \quad (4)$$

$$\mathbf{B} := b(\mathbf{X}) \quad (5)$$

as

$$T[f](\mathbf{X}) := \frac{1}{2\pi N_x N_y} \int_{x=0}^{N_x} \int_{y=0}^{N_y} \mathbf{A}(x, y) \int_{\varphi=0}^{2\pi} \mathbf{B}(x + |\vec{q}|\cos(\varphi), y + |\vec{q}|\sin(\varphi)) d\varphi dx dy \quad (6)$$

which then could be rewritten with a convolution (denoted as  $*$ ) as

$$T[f](\mathbf{X}) := \frac{1}{2\pi N_x N_y} \int_{x=0}^{N_x} \int_{y=0}^{N_y} \mathbf{A}(x, y) \cdot (\mathbf{B} * \mathbf{C})(x, y) dx dy \quad (7)$$

$$\text{where } \mathbf{C}(x, y) = \begin{cases} 1 & : \sqrt{x^2 + y^2} = |\vec{q}| \\ 0 & : \text{elsewhere} \end{cases}$$

This again is illustrated for one example in Figure 4.

A more general method to save computing costs has been described by Siggelkow and Schael (1999): the considered features are computed only approximately with the required precision.

Even though these features were designed to be only invariant to euclidian transformations, due to the finite kernel support they are additionally quite robust against other transformations like articulated motion or even slight topological deformations (Burkhardt and Siggelkow, 2001).

To adjust the gray scale invariants to a specific problem, one uses different kernel functions. This allows an easy construction of features that provide the required discrimination power. Using a small-scale kernel results in a feature which is sensitive to small-scale structures of the object. For example coarse or fine-grained plasm. Correspondingly large-scale kernels sense the large-scale structure of the object, e.g., the difference between spherical and ellipsoid objects.

For the pollen recognition we use just two kernel functions,

$$f_1(\mathbf{X}) = \mathbf{X}(0, 0, 0) \cdot \mathbf{X}(0, 0, 2) \quad (8)$$

$$f_2(\mathbf{X}) = \sqrt{\mathbf{X}(0, 0, 0)} \cdot \sqrt{\mathbf{X}(0, 0, 2)} \quad (9)$$

which are evaluated at 7 different scalings of the object (1:1, 1:2, 1:4, 1:8, 1:16, 1:32 and 1:64), resulting in a vector of 14 features that describe the object under consideration. Since the gray scale values of the input image were normalized to unit variance the elements

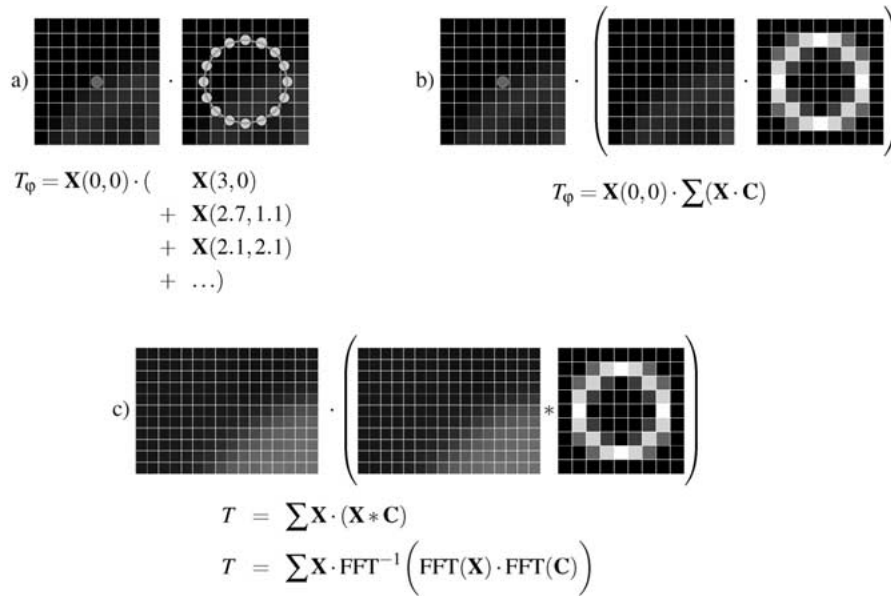


Figure 4. Fast calculation of a special class of gray scale invariants: (a) The sequential evaluation of the rotated kernel functions (as shown in Figure 3b) is split into two steps. Step 1: the gray values touched by the second kernel point within the rotation are summed up. Step 2: the result is multiplied with the gray value of the first kernel point. (b) step 1 could now be replaced by a pixel-wise multiplication with an image of a circle and the Integration of the results. (c) The evaluation of step 1 for all positions in the image is a simple convolution which could efficiently be calculated by means of the Fast Fourier Transform (FFT).

of the resulting feature vector are in the range  $[-1 : 1]$  corresponding to normalized correlation coefficients.

The 14 dimensional feature vector is computed for each object. Therefore each object is represented by one point in the 14-dimensional feature space. If the selected features were good, the points belonging to one class, e.g., all *Corylus*-pollen form a cluster which is clearly separated from clusters belonging to other classes. The task of the classifier is to decide to which of these clusters an unknown object belongs.

As a first approach we used the standard Mahalanobis-classifier, which models each of these clusters by a Gaussian probability distribution. So recognition rates of about 70% were achieved. A higher recognition rate is achieved by the so-called support vector machines (Vapnik, 1995) which we are using at present. The principal idea behind the support vector machine is to describe the clusters by searching for the thickest hyperplane, which separates this cluster from the remaining points. As the clusters are usually not linear separable (which means separable by a hyperplane in the original feature space) the points are transformed into a higher dimensional space, where they are linear separable. This transformation just leads to a redefinition of the distance function in the original feature space, which will be

expressed by means of a kernel function. The big advantage of support vector machines is, that they have an unambiguous global optimum and that the training process will find this optimum. Furthermore they are easy to handle, perform very well for low numbers of reference samples<sup>3</sup> and, last but not least, one can just download powerful and easy to use SVM implementations from the internet (e.g., Joachims, 2001). A good introduction to the theory of SVMs is given by C.J. Burges Tutorial (Burges, 1998).

### 2.5 Measuring the recognition rate

For measuring the quality of our recognition system, we have used a reference data base with the 26 most relevant German pollen taxa. 3D volume data sets of about 15 samples from each pollen taxon were recorded with a resolution of ca. 5 voxels/ $\mu\text{m}$  in each direction using a confocal laser scanning microscope with a 40x oil-objective, an excitation wavelength of 450–490nm and an emission wavelength greater than 510nm.

With these 385 high-quality volumetric pollen images we tested our recognition system using the “leave one out” technique. That means: the pollen grain to be classified was taken out and the classi-

fier was trained with the remaining 384 pollen grains. After that the left out pollen grain was classified with the resulting classifier. This was repeated for each pollen.

As classifier we use a set of 26 SVMs with a Gaussian kernel where each SVM was trained to separate one particular class from the rest. The radius of the Gaussian kernel was determined by optimizing the recognition rate.

### 3. Results and discussion

The recognition rate for all 26 taxa was about 92%. The details are listed in Table 1. There for each pollen taxon the number of correct and incorrect classifications are shown, where e.g., “1 → *Compositae*, 1 → *Platanus*” besides the *Artemisia* pollen means, that one of the *Artemisia* pollen was incorrectly classified as a *Compositae* and one was incorrectly classified as a *Platanus*.

For pollen forecasts we are only interested in the allergically relevant pollen. So it doesn't matter if the computer cannot distinguish, for example, between an *Ulmus* and a *Platanus*.

So we can put all these taxa into one class and end up with a recognition rate for allergically relevant pollen of 97.4%.

As one can see, the automatic recognition works nearly perfect on these high-quality pollen images. This high performance is encouraging enough to test the procedure with reduced data quality by using a normal fluorescence microscope with subsequent deconvolution (see Figure 5) and air samples with deformed or contaminated pollen. Last but not least we can use a pollen-calendar to reduce the reference data base to the seasonal possible set of pollen, which again should increase the recognition rate.

For establishing this system in a laboratory environment, one main aspect is the time needed for the evaluation. Currently the scanning with the LSM takes about 40s per object (depending on its size) and the calculation of the 14 gray scale invariants for a  $128^3$  voxel volume takes about 15s on a Pentium II Dual-Processor PC with 400MHz, so that we end up with a recognition time of about 1min for each object. This time will be dramatically reduced by using the normal fluorescence microscope, which can record the same 3D volume in a few seconds. On the computational side using a faster processor and perhaps reducing the resolution by a factor of 2 in each direction could

also reduce the recognition time to a few seconds per object.

Our current work also focuses on the 2D pre-recognition of the objects, so that only pollen with an unfavorable orientation or other doubtful objects have to be subjected to the relatively time-consuming 3D recognition.

On the other hand the time needed for the evaluation is less important for an on-line system because there it is sufficient to evaluate a one-day-sample within 24 hours.

### 4. Conclusions and outlook

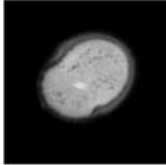
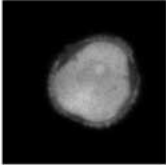
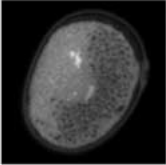
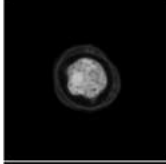
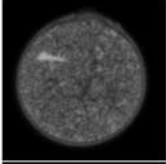
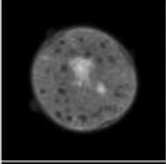
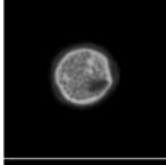
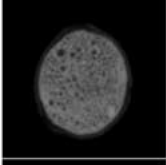
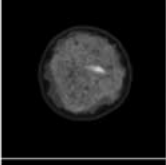
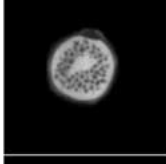
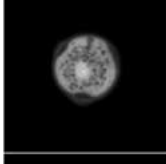
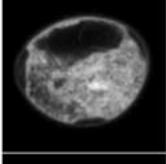
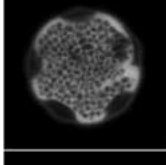
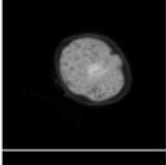
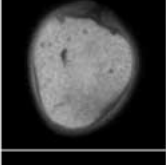
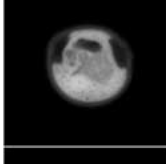
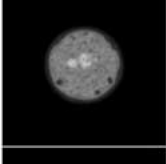
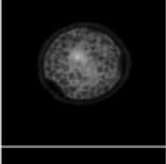
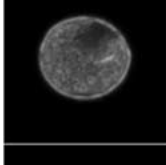
The utilization of fluorescence microscopy for the pollen recognition turned out to have considerable advantages in comparison to translucent microscopy. First it allows to isolate the pollen from the background and the other objects, and it allows a straight forward 3D volume analysis, because one can measure the local properties of the object largely independent from its orientation towards the direction of viewing and illumination.

The 3D information is required for a highly reliable pollen recognition even by a human, because a single 2D view of a pollen grain of unfavorable orientation does not contain sufficient information to realize an unequivocal classification.

The selected gray scale invariants turned out to be a powerful but simple to use approach for object recognition on 3D volume data. Up to now, there is no pollen-specific code in our recognition software, which makes it reusable for a wide range of other applications. The only limitation is that the objects have to be quite stiff within the support of the selected kernel functions.

It was demonstrated that our system can recognize pollen on the basis of 3D volume data with good reliability by using data recorded with a confocal laser scanning microscope, and pollen which are not deformed or contaminated. The recognition rate of 92% for all 26 pollen taxa and 97.4% when combining all allergically irrelevant in one class is encouraging, and gives reason to test the procedure with reduced data quality by using a conventional fluorescence microscope with subsequent deconvolution (see Figure 5) and air samples with deformed or contaminated pollen. We expect that the described approach may in near future replace the tedious and time consuming work of manual pollen counting.

Table 1. Classification results using 3D LSM data (leave-one-out classification)

|                                                                                     |                                                                                                     |                                                                                     |                                                                                                  |                                                                                      |                                                                                   |
|-------------------------------------------------------------------------------------|-----------------------------------------------------------------------------------------------------|-------------------------------------------------------------------------------------|--------------------------------------------------------------------------------------------------|--------------------------------------------------------------------------------------|-----------------------------------------------------------------------------------|
|    | <b>Acer</b><br>14 correct<br>1 → <i>Tilia</i>                                                       |    | <b>Cruciferae</b><br>13 correct<br>1 → <i>Acer</i><br>1 → <i>Populus</i>                         |    | <b>Secale<sup>(a)</sup></b><br>11 correct<br>3 → <i>Fagus</i><br>1 → <i>Tilia</i> |
|    | <b>Artemisia<sup>(a)</sup></b><br>13 correct<br>1 → <i>Compositae</i><br>1 → <i>Platanus</i>        |    | <b>Fagus</b><br>15 correct<br>no wrong                                                           |    | <b>Rumex</b><br>15 correct<br>no wrong                                            |
|    | <b>Alnus<sup>(a)</sup></b><br>15 correct<br>no wrong                                                |    | <b>Quercus</b><br>11 correct<br>1 → <i>Acer</i><br>2 → <i>Chenopodium</i><br>1 → <i>Plantago</i> |    | <b>Populus</b><br>14 correct<br>1 → <i>Chenopodium</i>                            |
|    | <b>Alnus viridis<sup>(a)</sup></b><br>12 correct<br>no wrong                                        |    | <b>Aesculus</b><br>15 correct<br>no wrong                                                        |    | <b>Salix</b><br>15 correct<br>no wrong                                            |
|   | <b>Betula<sup>(a)</sup></b><br>13 correct<br>2 → <i>Plantago</i>                                    |   | <b>Juglans</b><br>13 correct<br>1 → <i>Carpinus</i><br>1 → <i>Poaceae</i>                        |   | <b>Taxus</b><br>15 correct<br>no wrong                                            |
|  | <b>Carpinus</b><br>14 correct<br>no wrong                                                           |  | <b>Fraxinus</b><br>12 correct<br>2 → <i>Compositae</i><br>1 → <i>Plantago</i>                    |  | <b>Tilia</b><br>14 correct<br>1 → <i>Poaceae</i>                                  |
|  | <b>Corylus<sup>(a)</sup></b><br>13 correct<br>1 → <i>Alnus</i>                                      |  | <b>Plantago</b><br>13 correct<br>2 → <i>Fraxinus</i>                                             |  | <b>Ulmus</b><br>12 correct<br>2 → <i>Platanus</i><br>1 → <i>Populus</i>           |
|  | <b>Chenopodium</b><br>12 correct<br>1 → <i>Quercus</i><br>1 → <i>Plantago</i><br>1 → <i>Populus</i> |  | <b>Platanus</b><br>15 correct<br>no wrong                                                        |  | <b>Urtica</b><br>14 correct<br>1 → <i>Platanus</i>                                |
|  | <b>Compositae</b><br>15 correct<br>no wrong                                                         |  | <b>Poaceae<sup>(a)</sup></b><br>15 correct<br>no wrong                                           |                                                                                      |                                                                                   |

<sup>a</sup>Allergically relevant pollen.

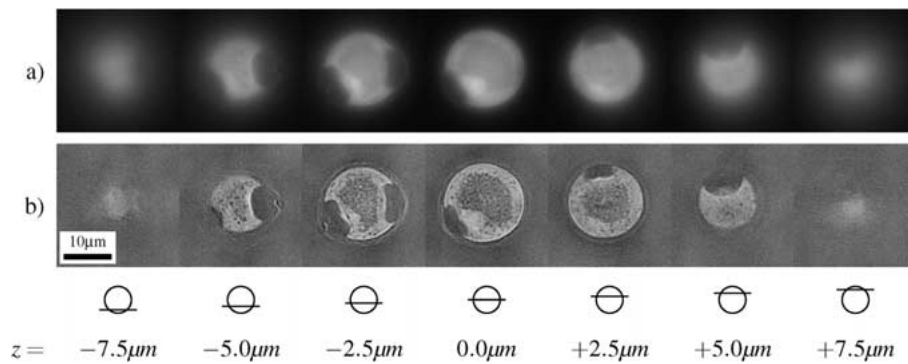


Figure 5. deconvolution (“software confocal”) applied to a fluorescence image stack of a *Corylus* pollen grain recorded with a 100x oil-objective and a conventional fluorescence microscope. In the original data (a) many details are nearly invisible due to the light originating from the parts of the pollen grain, which are out of focus. The deconvolution removes this light dispersion resulting in a clear image of each plane (b).

Furthermore, this approach opens up the possibility to directly integrate such a system into a pollen sampler resulting in an online pollen monitor.

More information concerning our project including some 3D volume images of pollen may be found on our web pages (Ronneberger, 2001).

### Acknowledgements

The authors would like to thank U. Heimann for the development of the image acquisition, microscopic automation and coordination of the reference data base setup. This work highly profited from the previous work of V. Dietze and his experience in automated image analysis on airborne particles. Furthermore we are grateful to S. Feigele and I. Huber for collecting and preparing the pollen, R. Nitschke and S. Haxelmanns for the LSM recordings and last but not least the MeteoSwiss for the financial and personal support for this project.

### Notes

1. Pixels = picture elements.
2. Voxels = volume elements.
3. The rule of thumb, that one needs at least three or more reference samples of one class per dimension of the feature space does not apply to them.

### References

Burges C.J.: 1998, A tutorial on support vector machines for pattern recognition. *Data Mining and Knowledge Discovery* **2**, 121–167.

- Burkhardt H. and S. Siggelkow: 2001, Invariant features in pattern recognition – fundamentals and applications. In: C. Kotropoulos and I. Pitas (eds), *Nonlinear Model-Based Image/Video Processing and Analysis*. John Wiley & Sons, pp. 269–307.
- France I., Duller A., Lamb H. and Duller G.: 1997, A comparative study of model based and neural network based approaches to automatic pollen identification. In: *British Machine Vision Conference*, pp. 340–349.
- Jain A.K.: 1989, *Fundamentals of Digital Image Processing*. Prentice-Hall.
- Joachims T.: 2001, *SVMLight, Implementation of Support Vector Machines in C*. [http://ais.gmd.de/~thorsten/svm\\_light/](http://ais.gmd.de/~thorsten/svm_light/).
- Langford M., Taylor G. and Flenley J.: 1986, The application of texture analysis for automated pollen identification. In: *Proceedings of a Conference on Identification and Pattern Recognition*. Toulouse, Univ. Paul Sabatini, pp. 729–739.
- Langford M., Taylor G. and Flenley J.: 1990, Computerized identification of pollen grains by texture analysis. *Review of Palaeobotany and Palynology* **64**, 197–203.
- Mazière M.: 1997, *Étude de faisabilité pour la reconnaissance automatique de grains de pollen*. <http://www-sop.inria.fr/orion/Publications/index.html>. Rapport de DEA, Université de Nice-Sophia Antipolis.
- McCrone W. and Delly J.: 1973, *The Particle Atlas*, Vol. IV. Ann Arbor Science Publishers, Ann Arbor, Michigan.
- Ronneberger O.: 2001, *Homepage of the Project ‘Automatic Identification and Counting of Airborne Pollen Grains’*. <http://bienemaja.informatik.uni-freiburg.de/pollen>.
- Schael M. and Siggelkow S.: 2000, Invariant grey-scale features for 3D sensor-data. In: *Proceedings of the International Conference on Pattern Recognition (ICPR2000)*. Barcelona, Spain, pp. 531–535.
- Schulz-Mirbach H.: 1995, Invariant features for gray scale images. In: G. Sagerer, S. Posch and F. Kummert (eds), *17. DAGM-Symposium ‘Mustererkennung’*, Informatik aktuell. Springer, pp. 1–14.
- Siggelkow S. and Schael M.: 1999, Fast estimation of invariant features. In: W. Förstner, J. Buhmann, A. Faber and P. Faber (eds), *Mustererkennung, DAGM 1999*. Bonn, Springer.
- Vapnik V.N.: 1995, *The Nature of Statistical Learning Theory*. Springer.

